

DETECTION OF HI IN EMISSION IN THE LYMAN ALPHA EMITTING GALAXY HARO 11

STEPHEN A. PARDY

Department of Astronomy, University of Wisconsin-Madison, 475 North Charter Street, Madison, WI 53706, USA

JOHN M. CANNON

Department of Physics & Astronomy, Macalester College, 1600 Grand Avenue, Saint Paul, MN 55105

GÖRAN ÖSTLIN

Department of Astronomy, Oskar Klein Centre, Stockholm University, AlbaNova University Centre, SE-106 91 Stockholm, Sweden

MATTHEW HAYES

Department of Astronomy, Oskar Klein Centre, Stockholm University, AlbaNova University Centre, SE-106 91 Stockholm, Sweden

NILS BERGVALL

Department of Physics and Astronomy, Uppsala University, Box 515, 751 20 Uppsala, Sweden

Draft version October 1, 2018

ABSTRACT

We present the first robust detection of HI 21 cm emission in the blue compact galaxy Haro 11 using the 100m Robert C. Byrd Green Bank Telescope (GBT). Haro 11 is a luminous blue compact galaxy with emission in both Lyman Alpha and the Lyman continuum. We detect $(5.1 \pm 0.7 \times 10^8)$ M_{\odot} of HI gas at an assumed distance of 88 Mpc, making this galaxy HI deficient compared to other local galaxies with similar optical properties. Given this small HI mass, Haro 11 has an elevated M_{H2}/M_{HI} ratio and a very low gas fraction compared to most local galaxies, and contains twice as much mass in ionized hydrogen as in neutral hydrogen. The HI emission has a linewidth of 71 km s^{-1} and is offset 60 km s^{-1} redward of the optical line center. It is undergoing a starburst after a recent merger which has elevated the star formation rate, and will deplete the gas supply in < 0.2 Gyr. Although this starburst has elevated the SFR compared to galaxies with similar HI masses and linewidths, Haro 11 matches a trend of lower gas fractions toward higher star formation rates and is below the general trend of increasing HI mass with increasing luminosity. Taken together, our results paint Haro 11 as a standard low-mass galaxy that is undergoing an unusually efficient star formation episode.

Subject headings: galaxies: ISM — galaxies: starburst — galaxies: kinematics and dynamics — radio lines: galaxies

1. INTRODUCTION

Haro 11 is a luminous blue compact galaxy (LBCG), a class of very bright and blue galaxies with intense star formation. Rare in the local universe (Werk et al. 2004), these LBCGs are typically gas rich (Garland et al. 2004) and likely form from merger events (Östlin et al. 2001; Bekki 2008). Haro 11 is a powerful emitter across the electromagnetic spectrum. It is classified as a Luminous InfraRed Galaxy (LIRG) with an infrared luminosity of $> 10^{11} L_{\odot}$, and shows signs of strong star formation likely due to a recent merger (Bergvall et al. 2000; Östlin et al. 1999, 2015). Haro 11 also shows emission in Ly α from some of its star forming regions (Hayes et al. 2007) and is one of a few currently known Lyman continuum emitting galaxies in the local universe (Bergvall et al. 2006; Leitet et al. 2013).

The detection of Ly α in emission in Haro 11 is particularly interesting. Ly α is an energetic star formation tracer that, in theory, can probe the stellar processing

in the early epochs of the universe. In practice, this line suffers from strong resonance scattering, uncertain extinction properties, and the fact that it is unobservable from the ground due to atmospheric absorption.

The scattering and extinction process is further complicated by a number of confounding factors. Dust content and properties alone cannot explain the observed extinction of Ly α (e.g. Giavalisco et al. 1996; Atek et al. 2009); instead, trends are apparent between the neutral gas content and geometry (Cannon et al. 2004; Kunth et al. 1998a). Super bubbles formed after star formation episodes can clear a path for escaping Ly α photons by shifting HI atoms into a different rest frame (Kunth et al. 1998b; Tenorio-Tagle et al. 1999). Ly α photons can also scatter while avoiding dust grains and spread into large halos (Hayes et al. 2013; Hayes 2015).

Many of these hypotheses are now being tested by targeted observations using the Hubble Space Telescope (HST; Wofford et al. 2013; Östlin et al. 2014). In particular, the Lyman Alpha Reference Sample (LARS; Östlin et al. 2014; Hayes et al. 2014; Pardy et al. 2014; Guaita

et al. 2015; Rivera-Thorsen et al. 2015) targeted 14 low- z potential Ly α emitters based on their ultraviolet luminosities and H α equivalent widths. Initial observations of the LARS galaxies with the HST were followed up with multi-wavelength observations of the gas and dust content, including neutral hydrogen in absorption (Rivera-Thorsen et al. 2015) and emission (Pardy et al. 2014). Combining observations of Ly α and H I emissions allow for direct comparisons and testing of the scattering effects at work. When combined with a dust tracer like H α /H β , this technique can also probe the extinction effects at work (Hayes et al. 2014).

Given its proximity and star formation intensity, Haro 11 is a prime candidate for studies of Ly α radiative transfer. The galaxy has three primary star forming knots A, B, and C (see Figure 1; Vader et al. 1993; Kunth et al. 2003; Adamo et al. 2010). One of these knots, knot C, shows Ly α emission, while the other two show absorption. This is striking because knots C and B have very similar dust content and extinction values (Atek et al. 2008). Further complicating matters, knot B has a stronger outflow of interstellar gas, yet no sign of Ly α emission (Sandberg et al. 2013).

Haro 11’s ISM properties have been extensively studied. Cormier et al. (2014) studied the molecular gas content of Haro 11 using both CO gas and IR dust emission. That work found a total H $_2$ mass of between 2.5×10^8 and 3.6×10^9 depending on the tracer used. James et al. (2013) used a variety of metallicity tracers to find a range of metallicities across the star forming knots from $12 + \log(\text{O}/\text{H}) = 8.25 \pm 0.15$ and $Z/Z_\odot = 0.35$ in Knot B, down to 8.09 ± 0.23 ($Z/Z_\odot = 0.24$) in Knot A, and 7.80 ± 0.13 ($Z/Z_\odot = 0.12$) in Knot C.

Yet, to date there has been no direct detection of 21 cm emission for Haro 11. Bergvall et al. (2000) first placed an upper limit on H I emission of $\leq 10^8 M_\odot$. H I was then seen in absorption by MacHattie et al. (2014), giving a mass range of $(3\text{--}10) \times 10^8 M_\odot$, with an upper limit on the emission of $M_{\text{HI}} \leq 1.7 \times 10^9 M_\odot$. This absorption measurement assumed a spin temperature between 91 and 200 K in the optically thin regime. In this paper we present the first robust detection of the H I spectral line in emission. In Section 2 we discuss the observations and data reduction. In Section 3 and Section 4 we present the results and interpret them in the context of LARS and other Ly α emitters.

Throughout this paper we assume a value of $H_0 = 70.2 \pm 1.4 \text{ km s}^{-1} \text{ Mpc}^{-1}$ (Komatsu et al. 2011).

2. OBSERVATIONS

We observed Haro 11 with the National Radio Astronomy Observatory 100m Robert C. Byrd Green Bank Telescope (GBT¹) in four 2.5 hour sessions under project 14B-306 (P.I. Pardy) with the VEGAS (Versatile GBT Astronomical Spectrometer) backend. The native resolution of the spectrum was 0.1 km s^{-1} . We obtained both XX and YY polarizations, which we averaged together for the final data.

All reductions were performed in the IDL environ-

¹ The National Radio Astronomy Observatory is a facility of the National Science Foundation operated under cooperative agreement by Associated Universities, Inc.

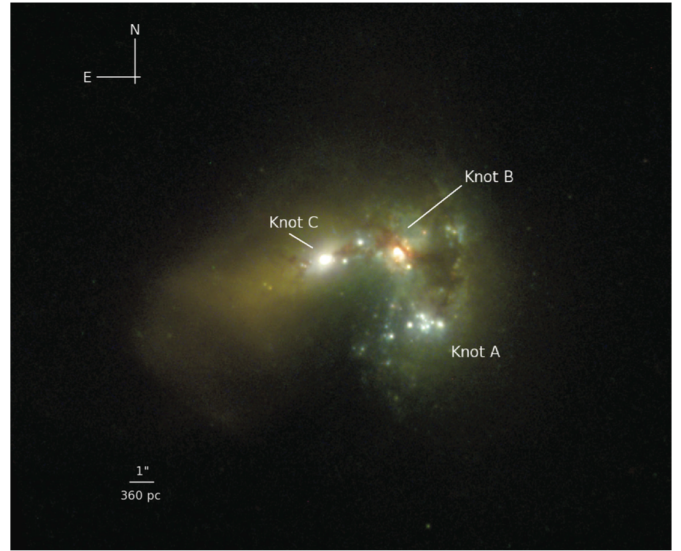


Figure 1. HST image of Haro 11 and its three primary star-forming knots. Figure from Adamo et al. (2010). Knot C is the only knot with Ly α emission, even though it shares very similar dust content with knot B (Atek et al. 2008), which also has a stronger outflow of interstellar gas (Sandberg et al. 2013).

ment², using the GBTIDL package designed at NRAO following the reduction strategy of Pardy et al. (2014). As in that work, we increase the Signal to Noise Ratio (SNR) by first averaging the reference spectrum by 16 channels. Then, adopting the baseline procedure of Leroy et al. (2008), we blanked all channels except for those within 400 km s^{-1} of either side of the emission peak. We then fit the unblanked channels with a first order baseline model and subtracted this model from all channels. Finally, we smoothed the spectrum to a resolution of 7.2 km s^{-1} .

We show the single dish H I spectrum in the top panel of Figure 2 centered near the systematic velocity. This Figure also illustrates our fitting and measurement routines. We fit a single gaussian component both to guide the reader’s eye, and to define the area over which to integrate the galaxy spectrum (gray line in Figure 2). Next we fit linear components to the sides of the emission (red lines) and take the width between these at 50% of the maximum value as the linewidth (blue line). The halfway point of this line is the galaxy centeroid (green line). This procedure was originally adopted from Springob et al. (2005) and discussed in more detail in Pardy et al. (2014). Pardy et al. (2014) also details our procedure for calculating measurement uncertainties. In brief, we use a conservative 10% uncertainty for baseline and calibration results, to which we add an uncertainty based on the width and noise of the spectrum:

$$\epsilon = rms \sqrt{W_{50} \times \Delta V}, \quad (1)$$

where ‘ rms ’ is the root mean squared noise of line-free channels, W_{50} is the width at 50% of the peak, and ΔV is the velocity resolution.

We use the single dish H I spectrum to measure the

² Exelis Visual Information Solutions, Boulder, Colorado

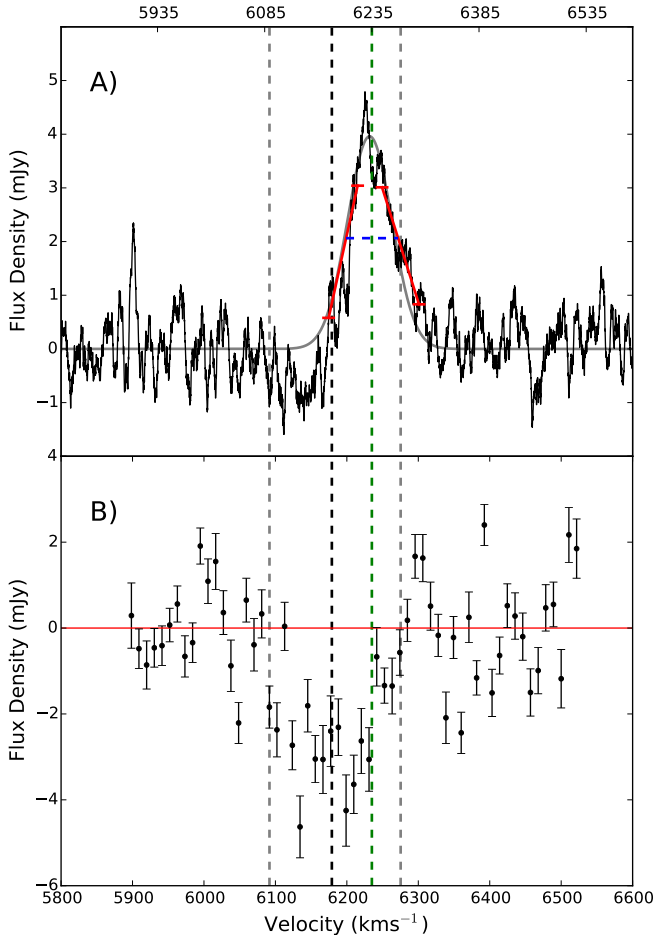


Figure 2. **A)** Single dish HI spectrum from the GBT. The spectrum is centered on the central velocity of 6236 km s^{-1} (vertical green dash line). The red solid lines show the fits to the sides of the spectrum used to measure the velocity width at 50% of maximum (horizontal blue dot-dash line). The solid gray line shows a single gaussian fit which is used to guide the eye and defines the velocity region to integrate over. The black and gray vertical dotted lines show the velocity center and total width of the absorption spectrum from MacHattie et al. (2014). **B)** HI absorption spectrum from MacHattie et al. (2014) (reproduced with permission from their figure 2). The solid black line shows their measured velocity of 6179 km s^{-1} .

total HI flux, and convert this to a mass using:

$$\frac{M_{HI}}{M_{\odot}} \approx 2.36 \times 10^5 \left(\frac{D}{\text{Mpc}} \right)^2 \int \left(\frac{S(\nu)}{\text{Jy}} \right) \left(\frac{d\nu}{\text{km s}^{-1}} \right). \quad (2)$$

Where D is the distance and S is the flux density. In this work we take the previous optical line center of 6180 km s^{-1} (Bergvall et al. 2006) and derive a Hubble-flow distance of 88 Mpc using the cosmology from Komatsu et al. (2011). This conversion from flux to mass assumes that the emission is optically thin, but does not require any knowledge of the spin temperature as is required by absorption-based masses. Using the derived mass and the known stellar mass we can then measure the fraction of neutral gas in the galaxy.

To ensure that this result was not due to the presence of contamination within the GBT beam, we checked the NASA Extragalactic Database (NED) for known galaxies within 30 arcminutes of Haro 11. No companions were

found.

3. RESULTS

Table 1
HI and stellar properties for Haro 11.

Stellar Properties		
Property	Value	Source
V_{opt}	6180 km s^{-1}	(Bergvall et al. 2006)
Distance	88 Mpc	(Bergvall et al. 2006) ^a
f_{esc}^b	0.037	(Östlin et al. 2009)
EW ^c	15.6 Å	(Östlin et al. 2009)
$Lum_{Ly\alpha}$	$8.4 \times 10^{41} \text{ erg s}^{-1}$	(Östlin et al. 2009)
SFR ^d	$24 M_{\odot} \text{ yr}^{-1}$	(Hayes et al. 2007)
M_{\star}	$9.4^{+12}_{-3.3} \times 10^9 M_{\odot}$	(Östlin et al. 2001)
M_{HI}	$10 \pm 1 \times 10^8 M_{\odot}$	(Bergvall & Östlin 2002)
$L_{B,\odot}$	$1.8 \times 10^{10} L_{\odot}$	(Bergvall & Östlin 2002) ^e
HI Properties (this work)		
Property	Value	
Flux	$0.28 \pm 0.04 \text{ Jy km s}^{-1}$	
V_{sys}^f	$6236 \pm 11 \text{ km s}^{-1}$	
M_{HI}	$5.1 \pm 0.7 \times 10^8 M_{\odot}$	
W_{50}	$77 \pm 21 \text{ km s}^{-1}$	
W_{20}	$125 \pm 33 \text{ km s}^{-1}$	
W_{max}^g	$163 \pm 42 \text{ km s}^{-1}$	
f_{gas}	$0.05^{+0.4}_{-0.4}$	

^a Using $H_0 = 70 \text{ km s}^{-1} \text{ Mpc}^{-1}$.

^b Escape fraction of $Ly\alpha$. ^c Equivalent width of $Ly\alpha$.

^d $H\alpha$ derived star formation rate. ^e Using distance = 88

Mpc. ^f Heliocentric radial velocity.

^g Full width of spectral line at zero-point crossing.

We measured the total flux of Haro 11 as $0.28 \pm 0.04 \text{ Jy km s}^{-1}$ at a velocity center of $6237 \pm 11 \text{ km s}^{-1}$ (using a heliocentric frame of rest). The un-smoothed spectrum has an rms noise of $3 \times 10^{-3} \text{ Jy}$ and a peak signal to noise ratio of 8. This line center corresponds to cosmological redshift distance of $89 \pm 2 \text{ Mpc}$. This central velocity is formally inconsistent both with the observed line center of $6179 \pm 16 \text{ km s}^{-1}$ found by MacHattie et al. (2014) and with the $H\alpha$ line center of 6146 km s^{-1} from James et al. (2013).

To test the validity of this detection, we split the dataset into the two separate polarizations and performed the analysis on each piece independently. We recover similar measurements from the two polarizations, all within our adopted uncertainties.

We compare the emission and absorption components in Figure 2. The absorption feature was unresolved in the observations of MacHattie et al. (2014), and comes from a region of size $< 3.54 \text{ kpc}$ near the center of Haro 11.

Using the total flux and a distance of 88 Mpc, we found a total of $5.1 \pm 0.7 \times 10^8 M_{\odot}$ of HI gas in Haro 11, which makes it an order of magnitude deficient compared to LARS galaxies with similar $Ly\alpha$ properties (see the left column of Figure 3), but in line with other starburst galaxies from Östlin et al. (2009). This HI mass is less than half the upper limit provided by MacHattie et al. (2014) and is ~ 5 times the order-of-magnitude limit provided by Bergvall et al. (2006). Due to the low HI mass, Haro 11 has a gas fraction (M_{HI}/M_{\star}) of 0.05 ± 0.4 , the lowest of any of the local comparison galaxies for which

HI was detected (see right column of Figure 3 and Section 4.1 for details).

We measure the velocity width at 50% of the peak emission as $77 \pm 21 \text{ km s}^{-1}$ and the velocity width at 20% of the peak emission as $125 \pm 32 \text{ km s}^{-1}$. Haro 11 has smaller linewidth than any LARS galaxies, as seen in the middle column of Figure 3. Our linewidth is narrower than the absorption derived HI linewidth of $112 \pm 16 \text{ km s}^{-1}$ (MacHattie et al. 2014). The total velocity extent is $163 \pm 42 \text{ km s}^{-1}$, formally consistent with those of MacHattie et al. (2014) and Östlin et al. (1999) (192 and 190 km s^{-1} respectively), and smaller than the H α derived value of 283 km s^{-1} from James et al. (2013).

Although Haro 11 appears to have less HI and a smaller linewidth when compared to galaxies in LARS with similar UV properties, none of these relationships, with the exception of the relationship between f_{esc} and linewidth, are significant. We quantify this by measuring Spearman's ρ coefficient (Spearman 1904), finding f_{esc} and linewidth with a correlation coefficient of -0.76 (p-value of 0.005). We next measured the strength of the correlation before and after including Haro 11 and looked for instances where the two properties became less correlated after the inclusion of Haro 11. In all cases, except for the relationship between gas fraction and EW^3 , the two variables became less correlated after including Haro 11.

4. DISCUSSION

4.1. Ly α Properties

We compare our observed HI mass, linewidth, and gas fraction for Haro 11 to the other starbursts from Östlin et al. (2009) and with galaxies from LARS (Hayes et al. 2014). Literature data for the HI properties of the Östlin et al. (2009) sample was compiled from a variety of sources and is presented in Table 2. We show all results in Figure 3. The rows show different Ly α properties

- **f_{esc} .** The Ly α escape fraction measured as the ratio of observed to intrinsic Ly α luminosity (Hayes et al. 2005, 2013) which was found in Pardy et al. (2014) to anti-correlate with total HI mass ($\rho = -0.62$). Shown in the top row of Figure 3.
- **EW.** The equivalent width of Ly α which was also found in Pardy et al. (2014) to anti-correlate with total HI mass ($\rho = -0.57$). Shown in the middle row of Figure 3.
- **Lum_{Ly α} .** The Luminosity of Ly α from Hayes et al. (2007, 2014). Shown in the bottom row of Figure 3.

Haro 11 does not follow the correlations seen in Pardy et al. (2014) for HI mass with f_{esc} (top left panel in Figure 3) and with EW (middle left panel in Figure 3), but one other starburst galaxy (Tol 65) is also nearly as offset as Haro 11 from the general trends. Haro 11 appears to also have a smaller linewidth (W_{50}) than LARS galaxies with similar f_{esc} and EW values, but this difference appears less pronounced than the offset with respect to HI

³ Although still not significant after the inclusion. Before including Haro 11: $\rho = 0.40$ (p-value = 0.22). After: $\rho = 0.45$ (p-value = 0.15).

mass. As discussed in Section 5, interactions are thought to facilitate the escape of Ly α photons, and often produce asymmetric line profiles and increased luminosities compared with isolated systems (Zaritsky & Rix 1997). Given that most of the LARS galaxies also showed signs of interactions, this may partly explain why the correlations between UV properties and HI linewidth were generally weaker than those with HI mass, and why Haro 11 falls within the linewidth scatter even with a dearth of HI.

In addition, the gas fraction seen in Haro 11 is nearly an order of magnitude smaller than any LARS galaxies as predicted by each of these three Ly α properties. The galaxies in Östlin et al. (2009) are generally smaller, with lower HI masses than the LARS sample ($5.9 \times 10^9 M_{\odot}$ for (Östlin et al. 2009) and $1.6 \times 10^{11} M_{\odot}$ for LARS). Because of this, these Ly α emitters appear as extreme as Haro 11 in these relationships. In particular, two of the galaxies IRAS 08339+6517 and NGC 6090 have lower gas fractions than the LARS galaxies (although they have masses and line-widths consistent with the larger sample; see the right column of Figure 3). Given the uncertain nature of the dependence on HI properties for the propagation of Ly α photons, a larger systematic study of HI properties in Ly α emitters is warranted. One such project is currently underway with the expanded Lyman Alpha Reference Sample (eLARS), which will increase the LARS sample by 28 galaxies (Melinder et al. in prep).

4.2. Relation to other Galaxies

Haro 11 has a stellar mass about one third that of the MW (Östlin et al. 2001; Licquia & Newman 2015), but a total mass near the upper limits of the LMC (Östlin et al. 2015; Peñarrubia et al. 2015) and an HI mass that is reminiscent of dwarfs. Because of this range of properties, we compare Haro 11 to a wide range of galaxy samples including regular star forming galaxies, dwarf galaxies, and galaxies selected for their similar blue colors or low metallicities as Haro 11.

Cormier et al. (2014) measured the H₂ mass of Haro 11 using both CO and dust tracers. Haro 11 appears to have a small CO flux, and using Galaxy scaled X_{CO} conversions gives $M_{H_2} = 2.5 \times 10^8 M_{\odot}$, whereas dust measurements give an estimate of $M_{H_2} = 3.6 \times 10^9 M_{\odot}$. Using these dust masses, a metallicity scaled X_{CO} provides a higher mass of $M_{H_2} = 2.5 \times 10^9 M_{\odot}$. Cormier et al. (2014) finds similar discrepancies between the CO and dust-derived H₂ masses for other galaxies in the Herschel Dwarf Galaxy Survey. All of the galaxies in their sample have faint CO lines and X_{CO} factors much larger than the Galactic value and therefore have uncertain H₂ masses. We can use this H₂ mass to derive an HI to H₂ mass ratio. Because there is such a large discrepancy between different methods, we choose to use the full range of H₂ masses reported by Cormier et al. (2014) in the analysis. This gives a range of $M_{H_2}/M_{HI} = 0.43 - 6.2$ depending on the mass of H₂ used.

If Haro 11 is indeed the product of a recent merger (Östlin et al. 2015), then comparisons with non-interacting galaxies may be biased. If we take these results at face value, however, we find that at the lower limit, Haro 11 has the fifth highest molecular gas fraction in this sample. At the higher limit it has a factor

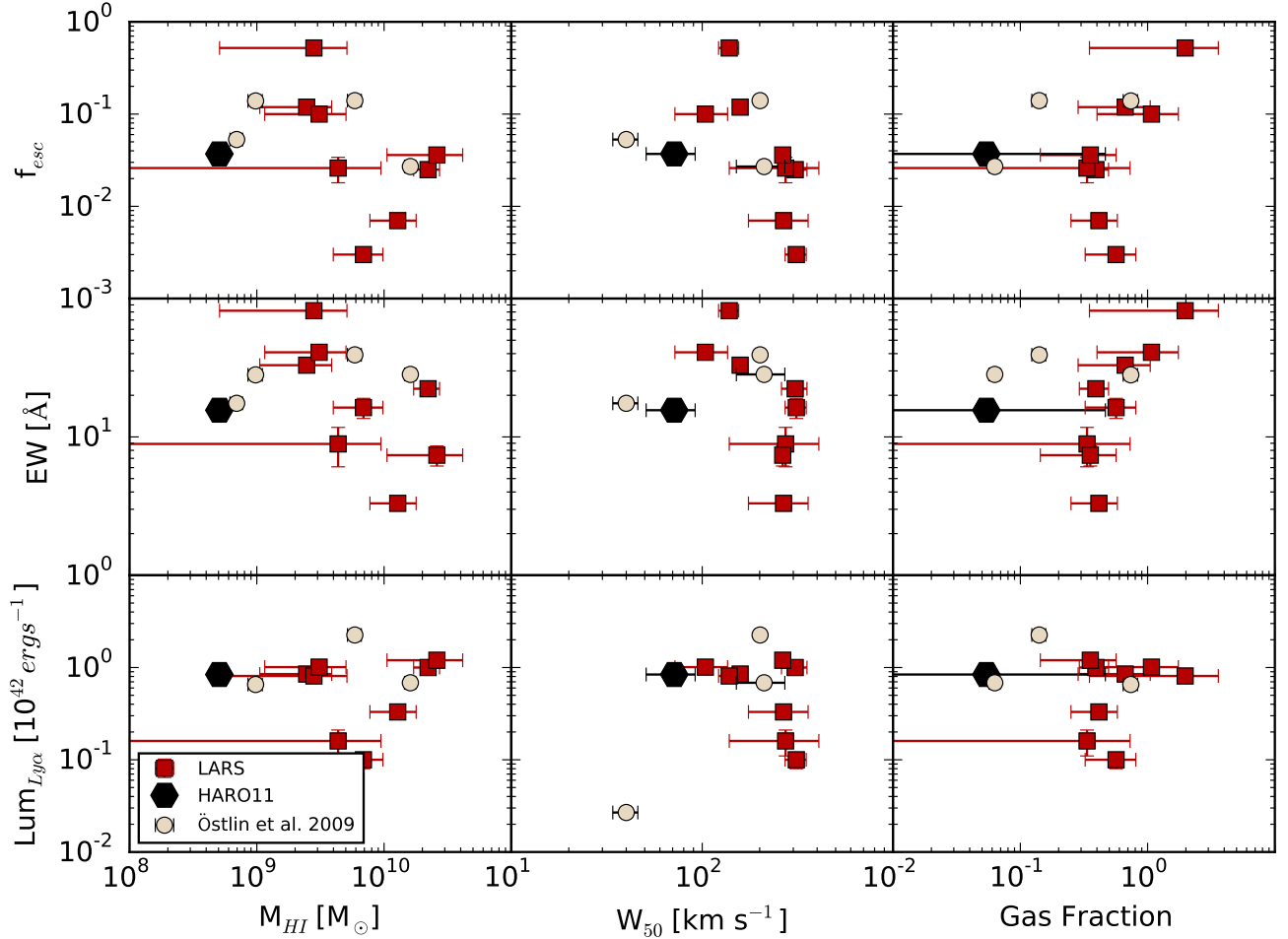


Figure 3. Ly α and HI properties of Haro 11 compared with other nearby starburst galaxies. In all panels Haro 11 is shown as a black hexagon, the LARS galaxies with clean detections are red squares, and the local starburst galaxies (see Table 2) are gray circles. Only galaxies with a positive Ly α luminosity are shown. Because of these quality and Ly α luminosity cuts, we do not show LARS 4, 5, 6, 12, 13, and 14. Each column shows a different HI property. *Left column:* HI mass. *Middle column:* linewidth at 50% of the line maximum. Note: ESO 338-04 is excluded from this panel because it has no published W_{50} value. *Right column:* gas fraction measured as M_{HI}/M_* . Note: Tol65 is excluded from this panel because it has no published M_* value. The rows show different Ly α properties. *Top row:* the escape fraction of Ly α . *Middle row:* the equivalent width of Ly α . *Bottom row:* Luminosity of Ly α

of seven higher ratio than any galaxies from the Heterodyne Receiver Array CO Line Extragalactic Survey (HERACLES; Leroy et al. 2009). See Figure 4. This large M_{H_2}/M_{HI} ratio is perhaps because infrared luminous galaxies are often seen with low atomic gas fractions (Mirabel & Sanders 1989).

In Figure 5 we compare the star formation and HI properties of Haro 11 to Luminous Compact Blue Galaxies (LCBGs) from Garland et al. (2004, 2005), to the HI in Nearby Galaxies Survey (THINGS) galaxies (Walter et al. 2008), and to LARS galaxies. The star formation rate for Haro 11 is measured from H α emission from Hayes et al. (2007). Haro 11 appears to be missing gas, both in terms of its low HI mass compared to other galaxies with similar SFR (left panel in Figure 5) and in terms of its narrow linewidth (middle panel). The gas fraction, however, paints a different picture. Haro 11 matches a trend of lower gas fractions toward higher star formation rates found in both the THINGS galaxies and the LCBGs (right panel of Figure 5). Taken together, these point to Haro 11 not as missing atomic gas, but as a stan-

dard low-mass galaxy that is undergoing an unusually efficient star formation episode. With an instantaneous H α SFR of $24 M_{\odot} \text{yr}^{-1}$ (Hayes et al. 2007), and the range of gas masses provided above (including a correction for primordial He), the gas will be depleted in 0.04-0.2 Gyrs.

Data from ALFALFA (Giovannelli et al. 2005), and HERACLES (Leroy et al. 2008), among others, have been used to demonstrate relationships between HI gas fraction and stellar mass (Papastergis et al. 2012; $\log F_g = -0.48 \log M_* + 4.39$) and between HI + H $_2$ gas fraction and stellar mass (Peeples et al. 2014; $\log F_g = -0.48 \log M_* + 4.39$) for normal star-forming disk galaxies. The general trend is that galaxies with smaller total stellar mass have a higher gas fraction. The HI mass in Haro 11 does not follow this prediction and, as seen in Figure 6, lies more than an order of magnitude below the trend. Haro 11 is interesting in this respect for two reasons. First, the HII mass is roughly twice the HI mass. Second, Haro 11 has a large H $_2$ /HI fraction. After assuming an upper limit of H $_2$ mass of $3.6 \times 10^9 M_{\odot}$, and $10 \times 10^8 M_{\odot}$ of ionized hydrogen, we can place Haro 11 on

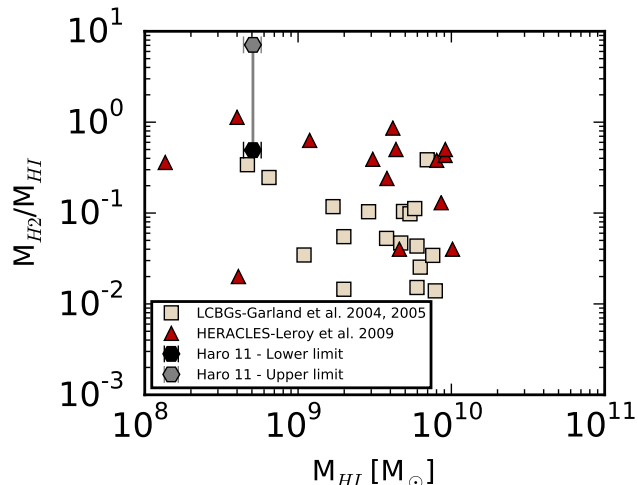


Figure 4. Molecular gas fraction, M_{H_2}/M_{HI} , for nearby galaxies and Haro 11. Comparison data is from the HERACLES sample (Leroy et al. 2008) (red triangles) and a sample of LCBGs from Garland et al. (2004, 2005) (gold squares). Haro 11 has an uncertain H_2 mass from Cormier et al. (2014). According to the CO derived mass, using a galactic X_{CO} , Haro 11 has $M_{H_2} = 2.5 \times 10^8 M_{\odot}$. The dust measurements, however, give an estimate of $M_{H_2} = 3.6 \times 10^9 M_{\odot}$. We show both points as an upper and lower limit to the M_{H_2}/M_{HI} ratio. At the lower limit, Haro 11 has the fifth highest molecular gas fraction in this sample. At the higher limit it has a factor of seven higher ratio than any HERACLES galaxies.

the $H I + H_2$ - stellar mass relationship found in Peeples et al. (2014).

Smoker et al. (2000) finds a trend in M_{HI}/L_B , with higher luminosity galaxies having lower gas ratios. We observe this trend in samples of BCDGs from Thuan et al. (2004) and Huchtmeier et al. (2007), a sample of LCBGs from Garland et al. (2004, 2005), a sample of extreme metal deficient dwarfs (XMDs; Pustilnik & Martin 2007), and with galaxies from THINGS (Walter et al. 2008). All galaxies from these papers have been corrected for our assumed cosmology wherever possible. Figure 7 shows how these galaxies match with the observed luminosity and HI mass of Haro 11. The right panel of Figure 7 shows the classic relationship of M_{HI}/L_B with M_B found in other papers, while the left panel shows a similar correlation of M_{HI} with respect to M_B . In both panels we include the transformation to luminosity in the top axis, assuming a solar B band magnitude of 5.48. The two relationships are highly correlated. The left and right panels have a Spearman’s correlation coefficient of -0.79 and 0.7 respectively and can be well described by simple power law fits ($\log_{10} M_{HI} = -0.3 M_B + 4.4$ and $\log_{10} M/L = -0.1 M_B + 2.2$). Haro 11 is a ~ 2 sigma outlier from the general trends (each relationship shows scatter of 0.46 dex), but is not the most extreme outlier.

4.3. Kinematics

The ISM kinematics of Haro 11 are highly irregular. The SiII line, seen in absorption by Kunth et al. (1998b), is blue shifted by 58 km s^{-1} from the optical line center. Sandberg et al. (2013) sees large velocity offsets between the ionized ($H\alpha$) and neutral gas (using a weak Na doublet line) that vary across the star forming knots. In Knot B, the neutral gas is blueshifted by 44 km s^{-1} ,

while in Knot C the neutral gas is redshifted by 32 km s^{-1} . Heckman et al. (2015) finds an outflow of 160 km s^{-1} using interstellar absorption lines in the warm ionized gas. Adding to this confusion, our HI emission line is redshifted nearly 60 km s^{-1} compared to the HI absorption (MacHattie et al. 2014) or $H\alpha$ emission (James et al. 2013) emission.

It is possible that we are seeing evidence of outflows carving cavities for the $Ly\alpha$ propagation. Such a phenomenon is seen in other irregular galaxies such as NGC 2366, which features two prominent outflows (van Eymeren et al. 2009). Although $H\alpha$ and HI kinematics are aligned across much of NGC 2366, the red-shifted $H\alpha$ outflow is in a hole in the neutral gas and has no HI counterpart.

Alternatively, the HI line in Haro 11 might be shifted due to large scale effects such as tidal tails. Such a tidal arm was proposed by Östlin et al. (2001, 2015) to explain a redshifted HII component. Although the measured HI velocity width is ~ 2.5 times narrower than the FWHM of the ionized gas, the ionized gas is multicomponent (Östlin et al. 2001). In particular Östlin et al. (2015) found a redshifted component with the same width ($\sigma = 30\text{-}25 \text{ km/s}$) as for the ionized hydrogen. They proposed that this component is a tidal arm. The HI that we see in emission could possibly be associated with this component, in which case it would not be associated with the main star formation site in the center (which is associated with the HI gas seen in absorption since the velocity matches and the width is consistent).

The total HI velocity extent is 160 km s^{-1} , which suggests another possibility. The outflowing gas we see might be right on the edge of the HI distribution and the bulk of this HI material might be simply behind the HII regions.

5. CONCLUSIONS

Haro 11 is a local starburst galaxy undergoing a major merger of two dwarf galaxies (Östlin et al. 1999, 2015). It has long been known to be a local $Ly\alpha$ -emitter, but until now has only had upper limits placed on its cold gas content. Our main contribution is the first robust detection of HI gas in emission from this blue compact galaxy consistent with previous upper limits (Bergvall et al. 2000; MacHattie et al. 2014). We find a dearth of HI gas and a linewidth at 50% of maximum that is smaller relative to other local starburst and LARS galaxies (Östlin et al. 2014; Hayes et al. 2014; Pardy et al. 2014).

Given the small HI mass, Haro 11 has an elevated M_{H_2}/M_{HI} ratio and a very low gas fraction compared to most local galaxies. Much of the hydrogen that remains has been heated during the merger process. Bergvall & Östlin (2002) derived a mass of $10 \pm 1 \times 10^8 M_{\odot}$ for the ionized hydrogen, twice as much as in neutral hydrogen. Haro 11 is undergoing an unusually efficient star formation episode, and matches a trend of lower gas fractions toward higher star formation rates and shares HI properties with galaxies of similar B-band magnitude.

Haro 11 is a known merging galaxy, which could explain the presence of tidal arms and complicated ISM kinematics. Two other merging local $Ly\alpha$ -emitters ESO 338-IG 004 (Tol 1924-416) and IRAS 08339+6517 were studied by Cannon et al. (2004) who found ex-

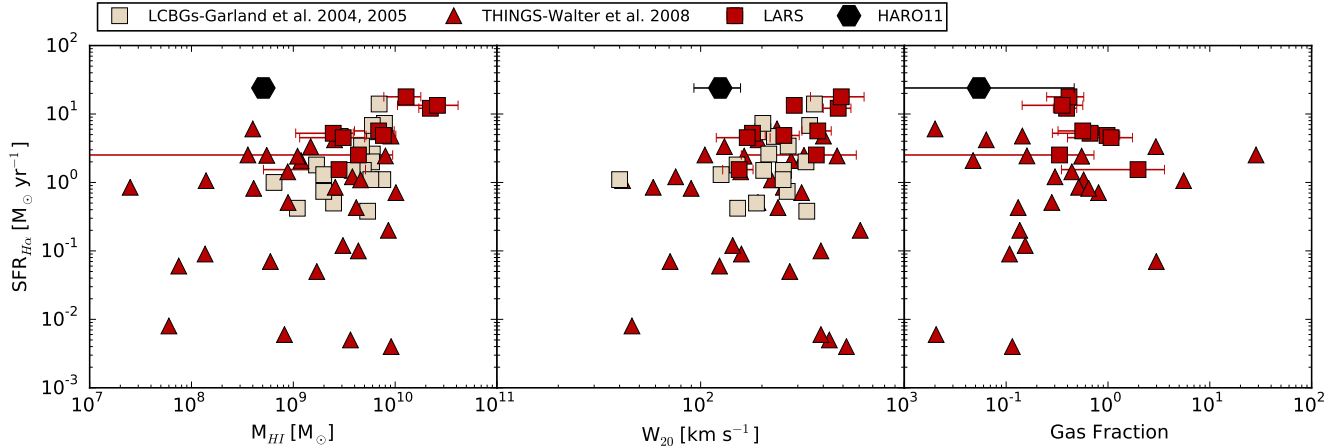


Figure 5. SFR and HI properties in Haro 11 and local galaxies. We compare with the LARS galaxies marked as clean detections (red squares), the THINGS galaxies (Walter et al. 2008) and other LCBGs from (Garland et al. 2004, 2005) (red triangles and gold squares, respectively). Because of the quality cuts, we do not show LARS 5, 6, 12, 13, and 14. *Left:* The HI mass shows that Haro 11 has an elevated SFR compared to other galaxies. *Middle:* The velocity width at 20% of the peak (W_{20}) of Haro 11 is less than would be expected from other galaxies. *Right:* The gas fraction (measured as M_{HI}/M_*) matches expectations of high star forming galaxies from these two samples.

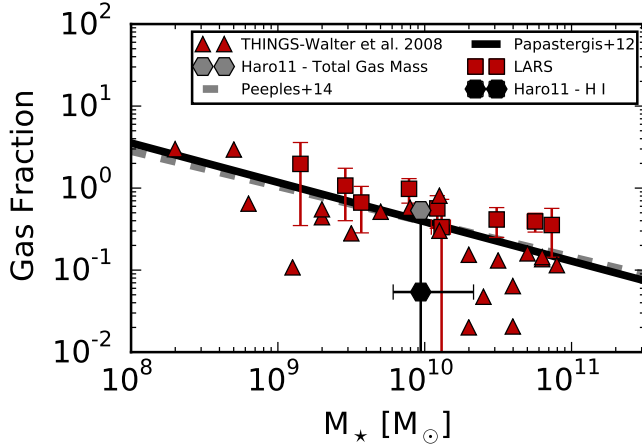


Figure 6. The relation between stellar mass and the gas mass fraction. LARS galaxies (Pardy et al. 2014) are converted from Salpeter to Chabrier IMF and are shown as red squares. THINGS galaxies (Walter et al. 2008) are shown as red triangles. We compare these galaxies and Haro 11, shown as a black hexagon and using a gas fraction derived only from the HI, to the relations found by Peeples et al. (2014) and Papastergis et al. (2012). The detections in the LARS sample, and many galaxies from THINGS, follow these predictions, but Haro 11 and four of the THINGS galaxies (IC 2574, NGC 3621, NGC 4449, and NGC 5055) lie an order of magnitude below the predicted gas fraction. The gray point shows the total gas fraction of Haro 11 (derived using the combined HI, H₂, and H α masses) compared with its stellar mass. This follows the predictions found in Peeples et al. (2014).

tended neutral gas connecting the main galaxy and companions. The processes that govern Ly α transport are complicated, but most often thought to involve the bulk motion of HI gas (Hayes 2015). Mapping the HI gas in emission across Haro 11 will be the only way to test these hypotheses, but this task remains a challenge for the current generation of radio telescopes. As we move to the high resolution HI era with the Square Kilometer Array (SKA), Haro 11 will be an excellent nearby target to probe the complicated coupling to cold neutral gas and Ly α propagation. Probing the three distinct star formation knots will reveal processes at work in enabling

Ly α escape.

This research made use of Astropy⁴, a community-developed core Python package for Astronomy (Astropy Collaboration, 2013). This research has made use of the NASA/IPAC Extragalactic Database (NED), which is operated by the Jet Propulsion Laboratory, California Institute of Technology, under contract with the National Aeronautics and Space Administration, and NASA’s Astrophysics Data System. SP thanks Jeremy MacHattie for providing the data for his figure 2 and for the discussion about his reduction methods. M.H. and G.Ö. acknowledge the support of the Swedish Research Council (Vetenskapsrådet) and the Swedish National Space Board (SNSB). M.H. is a Fellow of the Knut and Alice Wallenberg Foundation.

REFERENCES

- Adamo, A., Östlin, G., Zackrisson, E., et al. 2010, MNRAS, 407, 870
 Atek, H., Kunth, D., Hayes, M., et al. 2008, A&A, 488, 491
 Atek, H., Kunth, D., Schaerer, D., et al. 2009, A&A, 506, L1
 Bekki, K. 2008, MNRAS, 388, L10
 Bergvall, N., Masegosa, J., Östlin, G., et al. 2000, A&A, 359, 41
 Bergvall, N. and Östlin, G. 2002, A&A, 390, 891
 Bergvall, N., Zackrisson, E., Andersson, B. G., et al. 2006, A&A, 448, 513
 Cannon, J. M., Skillman, E. D., Kunth, D., et al. 2004, ApJ, 608, 768
 Cormier, D., Madden, S. C., Leboutteiller, V., et al. 2014, A&A, 564, 121
 Garland, C. A., Pisano, D. J., Williams, J. P., et al. 2004, ApJ, 615, 689
 Garland, C. A., Williams, J. P., Pisano, D. J., et al. 2005, ApJ, 624, 714
 Gialalisco, M., Koratkar, A., and Calzetti, D. 1996, Astrophysical Journal v.466, 466, 831
 Giovanelli, R., Haynes, M. P., Kent, B. R., et al. 2005, AJ, 130, 2598
 Guaita, L., Melinder, J., Hayes, M., et al. 2015, A&A, 576, A51
 Hayes, M. 2015, Publ. Astron. Soc. Aust., 32, e027

⁴ <http://www.astropy.org/>

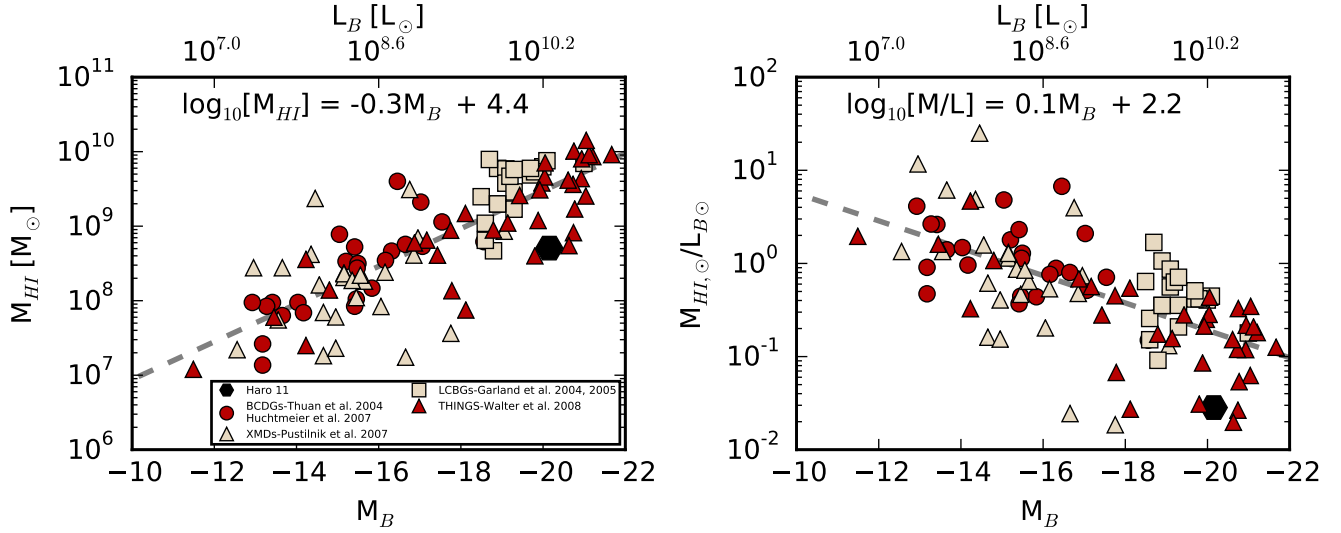


Figure 7. Comparison of HI mass with B band luminosity and magnitude. Comparison data in both panels is from BCDGs (Thuan et al. 2004; Huchtmeier et al. 2007) (red circles), XMDs (Pustilnik & Martin 2007) (gold triangles), LCBGs (Garland et al. 2004, 2005) (gold squares) and THINGS (Walter et al. 2008) (red triangles). *Left:* The M_{HI} with respect to M_B . We also include the transformed L_B in solar luminosities on the upper axis, assuming a B band magnitude of the sun of 5.48. Haro 11 is below the main trend, but sits with a few other THINGS galaxies. *Right:* The M_{HI}/L_B with respect to M_B . Although Haro 11 has a very low gas fraction compared to other BCDGs, LCBGs, and XMDs, it follows the general trend of decreasing mass-to-light ratio with increasing luminosity.

Hayes, M., Östlin, G., Atek, H., et al. 2007, MNRAS, 382, 1465
 Hayes, M., Östlin, G., Duval, F., et al. 2014, ApJ, 782, 6
 Hayes, M., Östlin, G., Mas-Hesse, J. M., et al. 2005, A&A, 438, 71
 Hayes, M., Östlin, G., Schaerer, D., et al. 2013, The Astrophysical Journal Letters, 765, L27
 Heckman, T. M., Alexandroff, R. M., Borthakur, S., et al. 2015, ApJ, 809, 147
 Howell, J. H., Armus, L., Mazzarella, J. M., et al. 2010, ApJ, 715, 572
 Huchtmeier, W. K., Petrosian, A., Gopal-Krishna, et al. 2007, A&A, 462, 919
 James, B. L., Tsamis, Y. G., Walsh, J. R., et al. 2013, MNRAS, 430, 2097
 Komatsu, E., Smith, K. M., Dunkley, J., et al. 2011, The Astrophysical Journal Supplement, 192, 18
 Kunth, D., Leitherer, C., Mas-Hesse, J. M., et al. 2003, ApJ, 597, 263
 Kunth, D., Mas-Hesse, J. M., Terlevich, E., et al. 1998a, A&A, 334, 11
 Kunth, D., Terlevich, E., Terlevich, R., et al. 1998b, arXiv, 9809096
 Leitert, E., Bergvall, N., Hayes, M., et al. 2013, A&A, 553, 106
 Leroy, A. K., Walter, F., Bigiel, F., et al. 2009, AJ, 137, 4670
 Leroy, A. K., Walter, F., Brinks, E., et al. 2008, AJ, 136, 2782
 Licquia, T. C. and Newman, J. A. 2015, ApJ, 806, 96
 MacHattie, J. A., Irwin, J. A., Madden, S. C., et al. 2014, MNRAS, 438, L66
 Martin, J. M., Bottinelli, L., Gougouenheim, L., et al. 1991, A&A, 245, 393
 Mirabel, I. F. and Sanders, D. B. 1989, ApJ, 340, L53
 Östlin, G., Amram, P., Bergvall, N., et al. 2001, A&A, 374, 800
 Östlin, G., Amram, P., Masegosa, J., et al. 1999, Astronomy and Astrophysics Supplement Series, 137, 419
 Östlin, G., Hayes, M., Duval, F., et al. 2014, ApJ, 797, 11

Östlin, G., Hayes, M., Kunth, D., et al. 2009, AJ, 138, 923
 Östlin, G., Marquart, T., Cumming, R. J., et al. 2015, A&A, 583, A55
 Papastergis, E., Cattaneo, A., Huang, S., et al. 2012, ApJ, 759, 138
 Pardy, S. A., Cannon, J. M., Östlin, G., et al. 2014, ApJ, 794, 101
 Peoples, M. S., Werk, J. K., Tumlinson, J., et al. 2014, ApJ, 786, 54
 Peñarrubia, J., Gómez, F. A., Besla, G., et al. 2015
 Pustilnik, S. A. and Martin, J. M. 2007, A&A, 464, 859
 Rivera-Thorsen, T. E., Hayes, M., Östlin, G., et al. 2015, ApJ, 805, 14
 Sandberg, A., Östlin, G., Hayes, M., et al. 2013, A&A, 552, A95
 Smoker, J. V., Davies, R. D., Axon, D. J., et al. 2000, A&A, 361, 19
 Spearman, C. 1904, The American Journal of Psychology, 15, 72
 Springob, C. M., Haynes, M. P., Giovanelli, R., et al. 2005, ApJS, 160, 149
 Tenorio-Tagle, G., Silich, S. A., Kunth, D., et al. 1999, MNRAS, 309, 332
 Thuan, T. X., Hibbard, J. E., and Lévrier, F. 2004, AJ, 128, 617
 Vader, J. P., Frogel, J. A., Terndrup, D. M., et al. 1993, AJ, 106, 1743
 van Driel, W., Gao, Y., and Monnier-Ragaine, D. 2001, A&A, 368, 64
 van Eymeren, J., Marcelin, M., Koribalski, B., et al. 2009, A&A, 493, 511
 Walter, F., Brinks, E., de Blok, W. J. G., et al. 2008, AJ, 136, 2563
 Werk, J. K., Jangren, A., and Salzer, J. J. 2004, ApJ, 617, 1004
 Wofford, A., Leitherer, C., and Salzer, J. 2013, ApJ, 765, 118
 Zaritsky, D. and Rix, H.-W. 1997, ApJ, 477, 118

Table 2
HI and stellar properties for local starburst galaxies.

Galaxy	EW (\AA)	$L_{\text{Ly}\alpha}$ ($\times 10^{41}$ erg s $^{-1}$)	fesc	M_{HI} ($\times 10^8 M_{\odot}$)	W_{50} (km s $^{-1}$)	M_{\star} ($\times 10^8 M_{\odot}$)
IRAS 08339+6517	39.2	22.4	0.140	59 ± 7.4 ^a	201 ^b	398.1 ^c
Tol 65	17.5	0.267	0.053	7.0 ± 0.80 ^d	40 ± 6 ^d	–
NGC 6090	28.3	6.79	0.027	160 ± 16 ^e	211 ± 60 ^e	2240 ^f
ESO 338-04	28.1	6.51	0.139	9.8 ± 1.3 ^a	–	12.6 ^c
LARS (Avg.)	21.69	0.91	0.09	1600	227	177

Note: $L_{\text{Ly}\alpha}$ and M_{HI} ($\times 10^8$) have been corrected for our cosmology. References: ^a Cannon et al. (2004)

^b Martin et al. (1991) ^c Leitert et al. (2013) ^d Pustilnik & Martin (2007) ^e van Driel et al. (2001)

^f Howell et al. (2010)